Main Manuscript for

Structural insights into peptidoglycan hydrolysis by the FtsEX system in *Escherichia coli* during cell division

Jianwei Li[1, #], Yutong He[1, #], Xin Xu[1, #], Martin Alcorlo[2], Jian Shi[3], Souvik Naskar[4], Nicholas S. Briggs[4], David I. Roper[4], Juan A. Hermoso[2], Lok-To Sham[5], and Min Luo[1, 3, *]

[1] Department of Biological Sciences, Faculty of Science, National University of Singapore

[2] Department of Crystallography and Structural Biology, Instituto de Química-Física "Blas Cabrera", CSIC, Madrid, Spain

[3] Center for Bioimaging Sciences, Department of Biological Sciences, National University of Singapore

[4] School of Life Sciences, University of Warwick, Coventry, CV4 7AL, UK

[5] Infectious Diseases Translational Research Programme and Department of Microbiology and Immunology, Yong Loo Lin School of Medicine, National University of Singapore

[#] These authors contributed equally.

* Corresponding author. Email : dbslmin@nus.edu.sg

Author Contributions: Jianwei Li and Yutong He performed biochemical reconstitution, functional characterization, and cryo-EM studies; Xin Xu performed kinetics assays; Souvik Naskar and Nicholas S. Briggs conducted co-purification studies of endogenous FtsA/FtsZ with FtsEX in *E. coli*. Martin Alcorlo, David Roper, Juan A. Hermoso and Lok-To Sham helped with data analysis; Jian Shi helped with EM data collection; Min Luo designed and supervised research, analyzed data, and wrote the paper with help from all authors.

Competing Interest Statement: Authors declare no competing interests.

Classification: Biological Sciences; Microbiology

Keywords: cell division, peptidoglycan, antimicrobial, cryo-EM

This PDF file includes:

Main Text

Figures 1 to 6

Abstract

Bacterial cell division relies on precise peptidoglycan (PG) remodelling, a process orchestrated by the FtsEX complex. Comprised of FtsE and FtsX, this complex collaborates with EnvC, a periplasmic lytic enzyme activator, to regulate septal PG hydrolysis by amidases like AmiB. While recent structural investigations, particularly of *Pseudomonas aeruginosa* FtsEX (*Pae*FtsEX), have shed light on complex interactions and proposed activation mechanisms, the structural intricacies governing PG degradation by the FtsEX complex and EnvC in *Escherichia coli* cytokinesis remain unexplored. In this study, we present a comprehensive biochemical and structural analysis of *E. coli* FtsEX complexes, unveiling a key role for ATP in complex stabilization that extends across bacterial species. Upon EnvC binding, ATPase activity markedly increases. High-resolution structures of *Eco*FtsEX, both in the presence and absence of EnvC, reveal a symmetrical conformation of *Eco*FtsEX capable of accommodating the inherent asymmetry of EnvC, mediated by flexible loops within the periplasmic domain. Our negative-staining imaging showcases an elongated *Eco*FtsEX/EnvC/AmiB complex reminiscent of the *Pae*FtsEX system. These findings collectively provide intricate insights into the regulation of PG cleavage by FtsEX in *E. coli* - a pivotal model system used in pilot genetic studies, suggesting a conserved mechanism for precise hydrolase activation in bacteria.

Introduction

In most bacteria, peptidoglycan (PG) remodeling during cell division is a precisely regulated process that ensures daughter cells separate without damaging the cell wall (1-3). This process involves a set of essential proteins that coordinate PG synthesis and degradation. In Escherichia coli, at least ten proteins contribute to cell division, many of which are organized by the cytoskeletal protein FtsZ (4, 5). FtsZ recruits FtsA and FtsEX to form the early divisome, a protein assembly at the division site. After a short delay, additional proteins, including FtsK, FtsQLB, FtsWI, and FtsN, are recruited to the septum (4, 6). The arrival of FtsN is a critical step that initiates cell constriction, likely through activating the FtsQLB complex and FtsA (4, 7-9). The final step in division, daughter cell separation, is carried out by PG-cleaving enzymes called amidases (AmiA, AmiB, and AmiC). These enzymes require activation by coiled-coil domain proteins: EnvC (which activates AmiA and AmiB) and NlpD (which activates AmiC) (1, 3, 10, 11). If these systems are simultaneously inactivated, the daughter cells will be unable to separate and form long chains (12).

PG remodelling is linked to cytokinesis by an ATP-binding cassette (ABC) transporter-like protein complex FtsEX. Rather than transporting a substrate, the FtsEX complex transduces conformational changes that span the cytoplasmic membrane (13, 14). Driven by ATP hydrolysis of FtsE, these changes are required for stimulating EnvC/AmiA/AmiB activities (15, 16) and

69 initiating cell constriction via FtsA (15, 17-19). The FtsEX complex also recruits other cell division
70 proteins to the divisome (17, 19). Thus, deletions of *ftsEX* result in non-viable cells unless they are
71 grown in permissive conditions, such as at a low temperature or in media with high osmolarity (20,
72 21). Alternatively, the essentiality of *ftsEX* can be bypassed by gain-of-function mutations that
73 strengthen the interaction between FtsN and FtsA (17, 20).
74
75 Several partial structures of the FtsEX complex have been reported, some are with their interacting
76 partners (22-25). Very recently, progress has been made in elucidating the full-length structure of
77 the FtsEX complex from *Pseudomonas aeruginosa* (*Pae*FtsEX), both in the presence and absence
78 of critical regulators like ATP, EnvC, and AmiB (26). These structures offer insight into the interfaces
79 between FtsE, FtsX, and their binding partners. In addition, they suggest a mechanism in which
80 the rearrangement of regulatory helices of EnvC and AmiB activates peptidoglycan hydrolysis at
81 the septum (26). Yet, the majority of work regarding FtsEX was done in *Escherichia coli* (15-21),
82 where an abundance of genetic studies has laid a significant foundation for our understanding of
83 PG degradation activation in bacterial cell division. However, the intricate molecular basis
84 orchestrating this process remains elusive, underscoring the need for a direct structural and
85 biochemical investigation within this extensively studied model system. Specifically, given the
86 relatively low sequence similarity between the FtsEX complexes from these two species, it is
87 unclear whether the structural information of *Pae*FtsEX can reconcile the findings from genetic
88 studies. Furthermore, previous genetic studies have proposed a direct interaction between FtsEX
89 and components of the constriction ring, such as FtsA and FtsZ (18, 27), to ensure the accurate
90 localization of FtsEX at the division site. However, there is currently a lack of supporting
91 biochemical and structural evidence in this regard.
92
93 In this study, we present a comprehensive analysis of the structure and function of the *Escherichia*
94 *coli* FtsEX complex (*Eco*FtsEX) in conjunction with EnvC, focusing on its regulation of AmiB
95 activation for PG cleavage. Our investigation uncovers a previously unrecognized function of ATP
96 in stabilizing the FtsEX complex, a role that appears to be conserved across different bacterial
97 species. Notably, we observe a substantial increase in the ATPase activity of *Eco*FtsEX upon
98 binding with EnvC. High-resolution structures of *Eco*FtsEX alone and with EnvC were obtained at
99 3.9 and 3.4 Å, respectively, offering insights into the EnvC recognition mechanism. Interestingly,
100 *Eco*FtsEX maintains a symmetrical conformation even when complexed with the asymmetrical
101 EnvC. Comparative analyses identify the periplasmic domain's flexible loops as key to EnvC
102 interaction, revealing structural adaptability. Furthermore, our negative-staining imaging
103 experiments unveil an elongated conformation of the *Eco*FtsEX/EnvC/AmiB complex for PG
104 cleavage, reminiscent of the FtsEX system from *Pseudomonas aeruginosa*. Together, our results

revealed a detailed regulation of PG cleavage by FtsEX in the key model system of *E. coli*, suggesting a conserved mechanism for hydrolase activation in bacteria.

Results

ATP Binding as a Universal Stabilizing Factor for the FtsEX Complex

In our efforts to reconstitute the full-length *Eco*FtsEX complex in vitro, we explored various strategies involving changing the expression constructs and extraction conditions. During the purification process, we observed that the protein remained stable in the presence of 10% glycerol. However, almost all protein precipitated out after the removal of glycerol either through size-exclusion chromatography (SEC) or during the peptidisc reconstitution (**Figure 1A**). This indicated a low level of stability for the complex. To investigate whether the stability of the FtsEX complex might be dependent on its cognate partner, EnvC, we conducted co-expression experiments by introducing EnvC along with FtsE and FtsX (**Figure 1A**). Despite the presence of EnvC, FtsEX still exhibited a tendency to precipitate.

Given the persistent challenges in achieving a stable FtsEX complex, we redirected our focus towards exploring the potential role of the substrate ligand, ATP, in complex stabilization. ATP, well-known for its role as a biological energy source, has also been associated with the stabilization of proteins, as reported in recent studies (28, 29). To investigate this hypothesis, we conducted a series of experiments to assess the impact of ATP on the FtsEX or the FtsEX/EnvC complex (**Figure 1A**). Remarkably, the introduction of ATP resulted in the formation of a robust *Eco*FtsEX complex, both in its standalone form and in the presence of EnvC. This complex remained tightly associated throughout the SEC process (**Figure supplement 1A**). Further validation through negative-staining electron microscopy confirmed that the purified *Eco*FtsEX complex maintained stability, with clearly discernible features corresponding to an intact ABC transporter containing two FtsE and two FtsX subunits (**Figure 1B**). This compelling evidence suggests that ATP, acting as the substrate of FtsEX, also plays a pivotal role in stabilizing this crucial complex formation.

Interestingly, ATP analogues, including ATPγS, AMP-PNP, and ADP, also exhibited similar stabilizing effects (**Figure 1C**). As they are not hydrolysable for FtsEX, it indicates that ATP binding, rather than hydrolysis, is sufficient for complex stabilization. This was corroborated by the introduction of a FtsE mutant (E163Q), inspired by related ABC transporters (26), which is incapable of ATP hydrolysis. When this mutant was assessed for complex formation with FtsX in the presence of ATP, it indeed formed a stable complex (**Figure 1C**). These findings suggest ATP binding alone is responsible for stabilizing the complex formation.

141 To expand the scope of our investigation, we explored whether ATP could similarly stabilize FtsEX
142 complexes from other bacterial species, which had also presented challenges in in-vitro
143 reconstitution. We expressed and purified FtsEX from various species, including *Streptococcus*
144 *pneumoniae, Pseudomonas aeruginosa*, and *Bacillus subtilis,* in the presence and absence of ATP.
145 Remarkably, regardless of the bacterial species, ATP consistently enhanced the stability of the
146 complexes, as demonstrated by either increased complex yield in SEC elution profiles or with a
147 more accurate stoichiometry between FtsE and FtsX as shown from the SDS-page gel (**Figure**
148 **supplement 1B**). Collectively, our findings underscore the pivotal role of ATP in stabilizing FtsEX
149 complexes. Notably, the ability of other nonhydrolizable ATP analogues to replicate this effect
150 suggests that ATP binding is a crucial step required to facilitate the coupling of FtsX and FtsE for
151 the formation of a functionally stable complex.
152
153 **Biochemical Characterization of FtsEX and Its Complexes with EnvC in *E. coli***
154 The His-tagged full-length FtsE and FtsX proteins from *E. coli* (str. K-12, MG1655) were
155 overexpressed in *E. coli* BL21(DE3) and subsequently purified using a combination of affinity and
156 size-exclusion chromatography (SEC) (**Figure supplement 1A**). For subsequent functional and
157 structural investigations, FtsEX was solubilized in DDM and reconstituted into peptidiscs (see
158 Methods). Given the proven stabilization role, 0.5 mM ATP was maintained throughout the entire
159 purification process of *Eco*FtsEX.
160
161 Assays assessing ATPase activity demonstrated that, in contrast to previously reported FtsEX
162 complexes from *Pseudomonas aeruginosa*, the *Eco*FtsEX complex exhibited obvious basal
163 ATPase activity (**Figure 1D**). To confirm this, we introduced the FtsE mutant (E163Q) as a control,
164 which was not able to hydrolyse ATP. As anticipated, ATPase activity in the mutant was markedly
165 diminished (**Figure 1D**), while low ATPase activity was still detected, potentially attributable to co-
166 purified proteins.
167
168 To understand the role of ATP binding/hydrolysis on EnvC recruitment, a protein pull-down assay
169 was conducted. As ATP was present in the purified protein, a wash step with buffer in the presence
170 of Mg^{2+} and 10% glycerol was performed to remove the extra ATP for the FtsEX complex that bind
171 to the resin. Next, bound FtsEX and EnvC were mixed in the presence of ATP or its non-
172 hydrolysable analogue, ATPγS (**Figure 1E**). The results revealed that EnvC stably associated with
173 FtsEX, with its binding seemingly unaffected by ATP hydrolysis. This was evidenced by the
174 comparable amounts of EnvC bound in the presence of 3 mM ATP, as well as its non-hydrolysable
175 analogs ATPγS and AMP-PNP, or even the hydrolysed product ADP. To confirm this, $FtsEX^{E163Q}$
176 mutant was introduced. Results, similar to those from the wild type, showed that the mutant still
177 demonstrated similar EnvC binding levels. The comparable binding of EnvC to FtsEX in the

178 presence of ATP, non-hydrolyzable analogs (ATPγS, AMP-PNP), and ADP suggests that ATP
179 binding is not required for EnvC recruitment to FtsEX, which aligns with multiple previous studies
180 that show the PLD domain of FtsEX is able to interact with EnvC in the absence of FtsE (30). This
181 indicates that EnvC association with FtsEX is nucleotide-independent and does not rely on ATP
182 hydrolysis. Instead, ATP binding likely plays a role in stabilizing the FtsEX complex, rather than
183 directly regulating EnvC recruitment.
184
185 Additionally, the effects of EnvC binding on the ATPase activity of *Eco*FtsEX were probed (**Figure**
186 **1D**). An enhanced activity was observed upon the addition of EnvC. This EnvC-mediated increase
187 in ATPase activity was further validated through ATPase assays involving varying ATP
188 concentrations for both FtsEX and the FtsEX/EnvC complex. Both sets of data fit well with the
189 Michaelis-Menten equation (**Figure 1F**). Notably, in the presence of EnvC, the V_{max} (92.7±5.1
190 nmol/mg/min) was approximately 2.2-fold higher than that observed for FtsEX (42.7±2.1
191 nmol/mg/min) alone. However, no large differences were observed regarding the K_m (0.11±0.02
192 mM for FtsEX/EnvC; 0.13±0.02 mM for FtsEX). Together, these findings underscore that in the
193 presence of ATP, FtsEX and EnvC form a robust complex; while *Eco*FtsEX inherently exhibits
194 ATPase activity, the presence of EnvC stimulates this activity.
195
196 **CryoEM structure of *Eco*FtsEX reveals a symmetrical PLD arrangement**
197 To elucidate the full-length structure of *Eco*FtsEX, we subjected the WT *Eco*FtsEX sample,
198 incubated with 3 mM ATPγS, to single-particle CryoEM analysis and achieved a resolution of 3.7 Å
199 (**Figure supplement 2**). This map was of sufficient resolution for detailed model-building for the
200 Transmembrane domains (TMD), the nucleotide-binding domains (NBD), and a large portion of the
201 Periplasmic domain (PLD); in addition, density for two bound nucleotides was clearly captured as
202 well (**Figure supplement 3A**).
203
204 *Eco*FtsEX, akin to most Type VII ABC transporters, possesses one coupling helice (CH) and a C
205 terminal tail (C-tail) (**Figure 2A**). Cryo-EM structure reveals the assembly of the full *Eco*FtsEX
206 system (**Figure 2B**). This comprises two cytosolic FtsE NBD domains and two FtsX, with TMD
207 domains embedded in the membrane and PLD extending into the periplasmic space. Both TMD
208 and NBD regions in the *Eco*FtsEX structure exhibit canonical folds, similar to other characterized
209 Type VII ABC transporters such as MacB, LolCDE, and *Pae*FtsEX. The overall conformation of
210 *Eco*FtsEX is quite similar to that of *Pae*FtsEX (**Figure supplement 3B**). Notably, the N-terminal
211 region of FtsX (Residues 53-70) forms an elbow helix (EH) oriented parallel to the membrane
212 (**Figure 2B**). Like its counterpart in *Pae*FtsEX, the extreme N-terminal region of FtsX (Residues 1-
213 52) was not resolved, suggesting its highly disordered nature.
214

The entire PLD domain comprises a smaller loop and a larger domain. For ease of reference, only the larger domain is termed the PLD (**Figure 2A**). The smaller loop encompasses 14 residues between TM3 and TM4. The principal PLD domain, spanning residues between TM1 and TM2 (106-208), displays a canonical topology, with a Porter domain and an X-lobe (14, 22). Compared to the TMD and NBD regions, PLD domains exhibit higher flexibility, evident from their diminished EM density at a contour level of 0.22 in Chimera. Lowering the contour to 0.1 in Chimera reveals clear density, enabling the visualization of PLD's secondary structures (**Figure supplement 2F**), with an exception for the X-lobe segment with residues 161-168 (**Figure 2C**). Structurally, the individual PLD domains are superimposable (**Figure 2C)**, and also align closely with those in *Pae*FtsEX (**Figure supplement 4**), despite their amino acid sequence identities with *E. coli* being only 29%.

The PLD domain of *Eco*FtsEX structure offers a snapshot with well-defined secondary structures, highlighting a 2-fold symmetrical conformation (**Figure 2D)**. The X-lobes of both PLDs are oriented mutually inwards with sideways blocked and appear to facilitate EnvC binding strictly from the top of the FtsEX complex, mirroring findings in the *Pae*FtsEX system.

CryoEM structure of *Eco*FtsEX/EnvC Complex elucidates EnvC binding and ATP-Dependent LytM Release

To elucidate the EnvC recruitment by FtsEX in *E. coli*, purified FtsEX^{E163Q} mutant was reconstituted in peptidiscs and incubated with EnvC in the presence of 2 mM ATP for cryo-EM analysis (**Figure supplement 5**). After 3D reconstruction, a major conformation stands out with resolution determined at 3.4 Å (**Figure supplement 5F**). The quality of the EM density allowed modelling of nearly all sidechains of FtsEX, the two bound nucleotides, and a portion of EnvC's coiled-coil domain (CCD) (**Figure 3A & Figure supplement 6**). The density of EnvC's remaining regions, including part of the CCD domain, the LytM domain and the regulatory helix, was absent, suggesting significant flexibility. The global configuration of the FtsEX/EnvC complex is similar to the previously described *Pae*FtsEX system (**Figure supplement 7**), where EnvC inserts from above between the two PLD domains along the FtsEX central axis.

To dissect the state of the bound EnvC, we compared our cryoEM FtsEX/EnvC complex with the crystal structure of the PLD domain in complex with EnvC (PLD/EnvC) from *E. coli* (PDB code: 6TPI) *(22)*, where EnvC was in an inactivated state. In the PLD/EnvC structure, a distinct asymmetrical conformation is evident: one PLD is positioned about 5 Å higher than the other one, accommodating the bound asymmetric EnvC with its LytM domain locked (**Figure supplement 8A, left**). However, in our full-length ATP-bound FtsEX/EnvC structure, the two PLDs are highly symmetrical (**Figure supplement 8A, right**). Besides this, the bound EnvC has also undergone

252 conformational shifts (**Figure supplement 8B**). In contrast to the PLD/EnvC crystal structure,
253 where the two CCD helices exhibit huge asymmetry (**Figure supplement 8B, left**), our structure
254 reveals a more symmetrical arrangement induced by simultaneous compression from both PLD
255 domains (**Figure supplement 8B, right**). Consequently, the distance between the terminal residue
256 of the α1 helix (Q127) and the initial residue of the α2 helix (Q143) within the CCD domain is
257 reduced from 24 Å to a mere 10 Å, while residing at a relatively similar height from the PLD domain.
258 This compression of the CCD helices may drive the release of the LytM domain, supported by the
259 lack of LytM density in our EM map. Together, we hypothesize that in the presence of ATP, the
260 LytM domain is released, facilitating AmiB recruitment.
261
262 **Comparison Between *E. coli* and *P. aeruginosa* FtsEX/EnvC Structures**
263 To further analyze the conservation and divergence of FtsEX/EnvC across species, we carefully
264 compared our newly determined *E. coli* FtsEX/EnvC structure with the previously reported *P.*
265 *aeruginosa* FtsEX/EnvC complex (**Figure supplement 9**). In both structures, the NBD domain
266 (FtsE) dimerizes upon nucleotide binding, forming a similar overall dimeric assembly. This is
267 coupled with a largely conserved conformation of the TMD domain (FtsX), with a root-mean-square
268 deviation (RMSD) of 2.05 Å across 386 α-carbons of FtsE and 2.64 Å across 349 α-carbons of the
269 FtsX TMD domain, indicating a high degree of structural similarity. Additionally, in both systems,
270 EnvC inserts into the PLD domain in a vertical conformation, further supporting a conserved mode
271 of interaction.
272
273 Despite these overall similarities, subtle differences exist between the two species. In *E. coli*, EnvC
274 binds even more vertical relative to the FtsEX axis, with about 5° difference compared to the
275 *Pae*FtsEX/EnvC structure. Along with this, a tighter coiled-coil (CC) conformation of *Eco*EnvC was
276 observed, accompanied by a further compressed X-lobe in *E. coli*. The X-lobes, tightly coupled to
277 the coiled-coil domains, appear to have been pushed further down toward the membrane in the *E.*
278 *coli* structure. This may, in turn, induce a more compact CCD domain in EnvC, explaining the tighter
279 conformation observed in *E. coli* compared to *P. aeruginosa*. These structural differences suggest
280 potential species-specific variations in EnvC recruitment or activation. However, given the limited
281 number of available FtsEX/EnvC structures, these conclusions remain preliminary. Additional
282 structures from other species will be required to determine whether these variations reflect
283 functional differences or simply structural plasticity within the FtsEX/EnvC system. Nonetheless,
284 our study provides key insights into the core architecture and conserved interactions of
285 FtsEX/EnvC, offering a structural framework for further investigations into bacterial cell division
286 regulation.
287
288 **Detailed EnvC interactions with FtsEX**

The ATP-bound *Eco*FtsEX/EnvC structure also revealed detailed interactions with EnvC. This interaction mainly involves two interfaces and covers an approximate surface area of 2290 $Å^2$, predominantly consisting of hydrophobic contacts (**Figure 3B**).

The primary interface, also resolved in the PLD/EnvC crystal structure (22), features residues Y114, F152, W155, F158, L162, L165, and L170 of FtsX associating with residues L117, L121, L148, Y151, F152, Y154, L155, and I163 of EnvC (**Figure 3C**). Conversely, the secondary interface encompasses the Lip of CCD from EnvC, and the small loop of FtsX. Interacting residues at this interface comprise I133, L135, I136, L137, E141 from EnvC and W210, L214, F309 from FtsX. Although hydrophobic interactions dominate, several electrostatic interactions exist, notably the salt bridges ($R126_{EnvC}$-$D207_{FtsX}$, $E141_{EnvC}$-$R213_{FtsX}$) (**Figure 3D**). These interactions have largely been validated by previous studies (22), mutations like Y114E, F152E, and L165A in FtsX's periplasmic domain notably affected EnvC's binding efficacy, affirming their role in recruiting EnvC.

Recognition of Asymmetrical EnvC by Symmetrical FtsEX: Unveiling Key Loops for Conformational Adaptivity

Intriguingly, our analysis of the FtsEX/EnvC structure showed that even when bound to the asymmetrical EnvC, FtsEX—including its two PLD domains interacting directly with EnvC—maintains a symmetrical conformation (**Figure 4A**). Compared to the *Eco*FtsEX structure without EnvC, which is also symmetrical, the only noticeable change is the outward shift of the two PLD hooks by about 12 Å (**Figure 4A**), a result of their interaction with the CCD domain of EnvC (**Figure 4B**). This observation poses an interesting question: How does the inherently symmetrical FtsEX cater to an asymmetrical binding partner? To explore this, we closely analysed the FtsX-EnvC binding interface.

Upon detailed examination, we noticed that the motifs in FtsEX directly interacting with EnvC are primarily loops (**Figure 4C**). The main loop engaging with EnvC is X-lobe (**Figure 4D**), covering residues G157-L171. This segment, originally disordered in the FtsEX alone structure, becomes crucial for engaging with EnvC, involving a binding interface of about 1204 $Å^2$. The other interacting regions are loops spanning residues Y104-Q109 (**Figure 4E**) and D208-L214 (**Figure 4F**), and a segment of the small loop in the PLD domain (Q307-T311) (**Figure 4G**). Combined, these loops (eight in total from the two PLD domains) are responsible for the majority of the interactions with EnvC. This inherent adaptability in the loops provides FtsEX the versatility needed for binding the asymmetrical EnvC. Notably, the interactions contributed by these loops are largely hydrophobic (**Figure 4D-G)**. Thus, our data suggest that the flexible loops, along with the hydrophobic interactions they facilitate, equip the symmetrical FtsEX to effectively engage with asymmetrical partners.

326

327 **Reconstitution and Elucidating the Elongated Conformation of *E. coli* FtsEX/EnvC/AmiB**
328 **Complex for PG cleavage**

329 The absence of the LytM density, in comparison to the crystal structure of PLD/EnvC (22), indicates
330 that our ATP-bound FtsEX/EnvC sample likely has the LytM domain released, primed for hydrolase
331 interaction. To further validate this, we conducted pull-down assays (**Figure 5A**). When we
332 incubated AmiB with either the FtsEX/EnvC complex or the mutant FtsEX^{E163Q}/EnvC in the
333 presence of ATP or its nonhydrolyzable analogue, ATPγS, both the wild type and mutant
334 FtsEX/EnvC complexes effectively pulled down AmiB. Notably, ATP and ATPγS showed similar
335 levels of AmiB binding, confirming that ATP-bound FtsEX/EnvC is prepped for AmiB recruitment.
336 Additionally, we investigated the influence of AmiB binding on FtsEX's ATPase activity (**Figure 5B**).
337 There was no obvious effect upon the addition of AmiB to the FtsEX/EnvC complex, suggesting
338 that AmiB does not regulate FtsEX function.

339

340 Next, we sought to check if the bound AmiB is activated for PG cleavage. FtsEX/EnvC complex
341 was first mixed with a threefold molar excess of AmiB in the presence of 2 mM ATP, and the mixture
342 was applied to size-exclusion chromatography (SEC) (**Figure 5C**). An early eluting fraction was
343 observed, and subsequent SDS-PAGE confirmed the co-existence of FtsE, FtsX, EnvC, and AmiB
344 in this fraction. The reconstituted PG-cleaving complex of *Eco*FtsEX/EnvC/AmiB, was further
345 analysed using negative staining (NS) electron microscopy (**Figure 5D**). Many of the observed
346 particles exhibited long tails in the image, a feature suggestive of AmiB binding. A 2D classification
347 analysis presented an elongated structure, mirroring previous observations in *P. aeruginosa* (26).
348 The electron densities on the periplasmic side displayed a distinct rod-like form in alignment with
349 the FtsEX complex's central axis, extending about 290 Å into the periplasm, which we attribute to
350 the bound EnvC and AmiB. This conformation likely represents an activated state prepared for PG
351 cleavage. However, due to the *Eco*FtsEX complex's instability during the PG hydrolysis assay, we
352 couldn't directly check PG cleavage activity. The attempt to obtain a CryoEM structure of the
353 complex was also unsuccessful, possibly because of its inherent flexibility, preventing the
354 reconstruction of a clear EM map. Nonetheless, it has been well established in *P. aeruginosa*,
355 where the active FtsEX/EnvC/AmiB complex also assumes an extended form (**Figure 5E**), we
356 propose that our observed complex with a similar conformation is also in an activated state, primed
357 for PG degradation.

358

359 **Discussion**

360 A structural and functional description is here provided for the complete *E. coli* lytic machinery
361 regulated by the FtsEX system. We observed an antiparallel arrangement of PLDs in the
362 periplasmic space in the *Eco*FtsEX complex. Incorporation of ATP, but not hydrolysis, is capable

363 of facilitating EnvC binding. The ternary complex increases its ATPase activity, compared with that
364 of the binary complex. Interestingly, upon ATP binding, the flexibility of loops in the PLD domain
365 allows a symmetric interaction with the EnvC coiled-coil domain that is compressed to allow the
366 release of its LytM domain. While resolution for the complete FtsEX/EnvC/AmiB complex limited
367 detailed descriptions, our cryo-EM data points to a very similar disposition of the lytic complex to
368 that reported for *P. aeruginosa* (26) with a fully expanded EnvC coiled-coil that would place the
369 amidase at ~300 Å over the inner membrane.
370
371 In the context of recruiting an asymmetric partner by the inherently symmetrical FtsEX complex,
372 our study has unveiled a dynamic and intriguing mechanism. At the centre of this mechanism lies
373 the highly flexible PLD domain (composed of the porter domain and the loops connecting the
374 different TM of FtsX), which demonstrates exceptional adaptability due to the presence of multiple
375 flexible loops, including the x-lobe. These flexible loops within the PLD domain function as dynamic
376 connectors, enabling the FtsEX complex to finely tune its conformation and engage with
377 asymmetric partners in an exceptionally adaptable manner. This inherent plasticity empowers the
378 FtsEX complex to align itself with the specific structural requirements of its binding partners, thereby
379 facilitating their effective interaction and subsequent regulatory processes.
380
381 Moreover, these flexible elements serve a dual role by providing the necessary adaptability to
382 bridge the gap between the inherent symmetry of the FtsEX complex and the asymmetry present
383 in its interacting partners. This becomes particularly intriguing in the context of bacterial cell
384 division, where the same FtsEX complex must interact with a variety of asymmetric binding
385 partners. These binding partners exhibit diverse structural features and distinct binding interfaces,
386 necessitating a mechanism that allows the inherently symmetrical FtsEX complex to engage with
387 them with precision and effectiveness.
388
389 Our study has uncovered a previously unrecognized role of ATP in the stabilization of the FtsEX
390 complex, a role that extends beyond its established function as a substrate. This discovery not only
391 expands our understanding of the functional versatility of ATP but also unravels a crucial aspect of
392 how FtsEX complexes are regulated. The stabilizing influence of ATP is particularly intriguing, as
393 evidenced by our experiments across diverse bacterial species, suggesting that ATP-driven
394 stabilization might represent a shared feature among FtsEX complexes in various bacteria.
395 Furthermore, it is noteworthy that both the FtsEX systems from *E. coli* and the recently
396 characterized system from *P. aeruginosa* exhibit a relatively low basal ATPase activity. However,
397 this activity is significantly enhanced in the presence of their respective cognate binding partner,
398 EnvC. Specifically, for *E. coli*, the ATPase activity increases by a factor of 2.2, whereas for *P.*
399 *aeruginosa*, the increase is even more pronounced, with a greater than 20-fold enhancement

400 observed. This additional regulatory mechanism ensures that, under normal physiological
401 conditions, minimal energy is expended. It is only during the cell division process, when
402 components like EnvC are involved, that the ATPase activity of FtsEX becomes fully activated.
403
404 Interestingly, our cryoEM map of *Eco*FtsEX, expressed from its native host bacteria *E. coli*,
405 revealed an additional density located on the bottom side of the complex adjacent to FtsE (**Figure**
406 **supplement 2**, and **Figure supplement 10A**). This suggests the co-purification of endogenously
407 binding proteins with the complex. To identify the proteins, we conducted mass spectrometry on
408 the purified FtsEX sample. Our results showed that in addition to FtsE and FtsX, FtsA was present
409 in significant abundance, followed by FtsZ (**Figure supplement 10B**). This observation is
410 consistent with previous genetic and phenotypic observations on the *E. coli* divisome activation
411 (17, 27). We also noted during the course of these studies that the interaction of *E.coli* FtsA with
412 FtsEX protein complexes from other species is indicative of the conserved and fundamental nature
413 of divisome protein interactions. For example, the overexpression of *S. pneumoniae* FtsEX in *E.*
414 *coli* also indicated an association with *E.coli* FtsA and could be isolated using styrene-maleic acid
415 isolation and affinity purification as shown in **Figure supplement 10C** (31, 32). If this holds true, it
416 would provide a mechanism for the temporal regulation of PG cleavage at the cell division site, as
417 FtsA and FtsZ are the key components of the constriction ring at the septum site (15, 18, 27, 33-
418 37). However, the identity of this density and the association of FtsEX with other Fts components
419 for divisome formation warrant further investigation to fully elucidate the role of FtsEX in bacterial
420 cell division.
421
422 In combination with previous studies on the inactivated EnvC (22) and AmiB activation by
423 *Pae*FtsEX (26), we propose a working model that may be conserved across Gram-negative FtsEX
424 systems (**Figure 6**). Firstly, physiological ATP stabilizes the formation of a functional FtsEX
425 regulator with low basal ATP hydrolysis activity; In the periplasm, the inactive EnvC interact with
426 the flexible PLD domain of FtsEX, which adopts a highly asymmetric conformation, as shown in the
427 inactivated EnvC structure (22). Our study, along with previous findings, highlights the crucial role
428 of ATP binding in stabilizing FtsEX, likely by promoting FtsE dimerization in the cytosol. Meanwhile,
429 EnvC binding plays a key role in stimulating FtsEX ATPase activity. Although EnvC binding appears
430 nucleotide-independent, the precise sequence of ATP binding and EnvC recruitment during cell
431 division remains to be further explored. Next, upon full recognition by FtsEX, considering the
432 presence of ATP in cell and a symmetrical conformation defined within the context of a full-length
433 FtsEX complex, recruited EnvC is compelled to adopt a relatively symmetrical conformation,
434 involving squeezing of the coiled-coil domain to facilitate the release of the LytM domain. Finally,
435 the released LytM recruits amidases through direct interaction, consequently removing the blocking
436 helix from the catalytic site and activating PG cleavage. Remarkably, expansion of the coiled-coil

437 domain in EnvC would place the amidase domain ~300 Å over the inner membrane of the Gram-
438 negative bacteria (as here seen in *E. coli*, and also in *P. aeruginosa* (26)), compatible with the
439 location of the septal PG (26) and avoiding damages into the non-septal cell wall. Throughout this
440 process, ATP binding appears to be sufficient, with ATP hydrolysis potentially serving as a driving
441 force for the release of EnvC and amidases from FtsEX, allowing them to be recycled to a normal
442 ABC transporter. This transporter by itself may play additional roles, such as antibiotic resistance,
443 as suggested by previous studies (22). For the temporal regulation of PG cleavage, the potential
444 interaction between FtsEX and FtsA/FtsZ, as indicated in this study and previous genetic research
445 (17, 27), could bridge the PG-cleaving complex with septum constriction ring, facilitating precise
446 cell division at the septum site. This model provides a potential conserved mechanism for PG
447 cleavage activation by FtsEX and illuminates its temporal regulation. Although further validation is
448 required, our results offer valuable biochemical and structural insights that complement and
449 elucidate decades of genetic research in *E. coli* and other Gram-negative bacteria.
450

451 **Materials and Methods**

452 **Cloning and Mutagenesis**

453 The primers and templates utilized in this study are listed in **Table supplement 1**. To generate the
454 PCR amplicon containing FtsEXs in genomic DNA of *Escherichia coli* Str *K-12 MG1655*,
455 *Streptococcus pneumoniae str. D39*, *Bacillus_subtilis_subsp_subtilis_ATCC_23857*, and
456 *Pseudomonas aeruginosa ATCC 47085D*. ClonExpress II One Step Cloning Kit (Vazyme) was
457 used, followed by purification. After purification through gel electrophoresis, the resulting product
458 was ligated to pTD68 vector (PMID: 20300061) digested with the Nde I and Hind III enzymes to
459 produce pTD68 [PT7::his6-FtsEX]. The construction of pET28-sumo (PT7:his6-sumo-
460 *Eco*EnvC∆34), (PT7:his6-sumo-*Eco*AmiB∆22), involved ligating pET28-sumo digested with BamH
461 I and Xho I to a PCR amplicon synthesized by EnvC-F, EnvC-R, AmiB-F, AmiB-R which were also
462 digested with the same enzymes. The plasmids utilized in this study are listed in **Table supplement**
463 **2.** Mutations to *Eco*FtsE was generated utilizing the QuikChange kit (Agilent Technologies), using
464 pTD68 and pET28-sumo as templates and the primers listed in **Table supplement 1**. The
465 mutations were then verified by DNA sequencing.
466

467 **Protein expression, purification of FtsEX complex and their mutants**

468 FtsEX and its mutants are expressed in *E. coli* strain BL21(DE3) pLysS (Invitrogen) using lysogeny
469 broth (LB) supplemented with 50 µg/ml ampicillin and 10 µg/ml chloramphenicol. This is incubated
470 at 37°C until an optical density at 600 nm (OD_{600}) of 0.8 is achieved. Following this, induction with
471 0.5 mM isopropyl-β-D-thiogalactoside (IPTG) takes place at 20°C for 16 hours. The cells are
472 subsequently harvested through centrifugation using a Beckman JLA9-1000 rotor at 5,180 xg and
473 20°C for 15 minutes. Harvested cells are then stored at -80°C.

474

475 For membrane extraction, the frozen cell pellets undergo thawing at 4°C and are resuspended in
476 buffer A, consisting of 50 mM Tris-HCl pH 8.0, 250 mM NaCl, 10% glycerol, and 2 mM ATP/$MgCl_2$.
477 Lysis of the mixture was achieved with a high-pressure homogenizer (AH-100D, ATS). Subsequent
478 centrifugation was performed at 27,000 xg for an hour at 4°C. Following this, solubilization of the
479 membrane takes place in buffer B, containing 50 mM Tris-HCl, 250 mM NaCl, 1.3% n-dodecyl β-
480 D-maltoside (DDM), pH 8.0, 10% glycerol, and 2 mM ATP/$MgCl_2$, and agitated for 2 hours at 4°C.
481 Post a 30-minute centrifugation at 100,000 xg, the solubilized membrane fraction gets incubated
482 with TALON SuperFlow resin (Takara 635502) for 1 hours at 4°C and was later washed using buffer
483 B supplemented with 20 mM imidazole. The present detergent is substituted by a peptide
484 (GenScript) to form peptidiscs, employing the "on-beads" method (38, 39) with a final peptide
485 concentration of 1mg/ml. The FtsEX complex, reconstituted in the peptidiscs, is washed using
486 buffer B inclusive of 20 mM imidazole and eluted with buffer B rich in 200 mM imidazole. The
487 purified protein is directed through a gel filtration chromatography column (Superose 6 increase
488 10/300) and is eluted with buffer C, which includes 25 mM Tris-HCl, 150 mM NaCl, pH 8.0, and 2
489 mM ATP/$MgCl_2$. The fractions bearing the FtsEX complex are combined together, concentrated to
490 3 mg/ml by concentrator (Amicon® Ulyra-15 100kDa), and preserved at -80°C for further protein
491 interaction, pull-down, and ATP hydrolysis assay.
492

493 **Protein expression, purification of EnvC, AmiB**

494 For the expression of EnvC, AmiB and their respective variants, the *E. coli* strain BL21(DE3) pLysS
495 was employed. These cells were cultured in LB medium with 50 μg/ml kanamycin at 37°C. Once
496 the OD_{600} reached a value of 0.6, induction was facilitated by the addition of IPTG to achieve a final
497 concentration of 0.5 mM, and this was maintained for 16 hours at 20°C. Following the induction,
498 cells were harvested through centrifugation using a JLA9-1000 rotor in a Beckman centrifuge at
499 5,000 rpm and 20°C for a duration of 15 minutes. The resulting pellets were stored at -80°C. For
500 further processing, these frozen pellets were brought to 4°C for thawing, using buffer C (50 mM
501 Tris-HCl pH 8.0, 150 mM NaCl, and 10% glycerol) and then subjected to lysis via a high-pressure
502 homogenizer (AH-100D, ATS). Subsequent centrifugation was performed at 27,000 xg for an hour
503 at 4°C. The resultant supernatant was incubated with TALON resin, followed by a wash using buffer
504 C complemented with 20 mM imidazole. Post-washing, the His-tagged SUMO protease Ulp1 was
505 introduced to the resin-buffer at a ratio of 0.1 mg Ulp1 for every liter of culture, facilitating the
506 cleavage of the SUMO tag over 2 hours at ambient temperature. The processed samples were
507 isolated, concentrated, and then passed through the Superose 6 increase 10/300 column
508 previously balanced in buffer D which includes 25 mM Tris-HCl, 150 mM NaCl, pH 8.0. Target
509 protein was confirmed using SDS-PAGE, further concentrated up to 3 mg/ml, and stored at -80°C.
510

511 **Analyzing the Impact of ATP on the FtsEX Complex**

512 Expression and purification of FtsEXs which from *Escherichia coli (Eco)*, *Streptococcus*
513 *pneumoniae (Sp)*, *Bacillus_subtilis (Bs)*, and *Pseudomonas aeruginosa (Pae)* followed the
514 procedure above. For the ATP-free FstEXs purification, the whole process excludes ATP. For the
515 samples of FtsEXs with ATP or ATP analogs, 2 mM ATP or ATP analogs present in the purification
516 process. The processed samples of *Sp*FtsEX, *Bs*FtsEX, *Pae*FtsEX were concentrated, and then
517 passed through the Superose 6 increase 10/300 column previously balanced in buffer which
518 includes 25 mM Tris-HCl, 150 mM NaCl, pH 8.0 with or without 2 mM ATP. The eluted proteins
519 profiles were confirmed using SDS-PAGE gel. For the *Eco*FtsEX/EnvC samples purification add
520 EnvC with final concentration 1mg/ml after FtsEX reconstituted in the peptidiscs. The eluted ATP-
521 free *Eco*FtsEX sample was performed at 12,000 xg for 15 min at 4°C due to persistent precipitate
522 appearing in the eluted sample. Confirming the supernatant and precipitate using SDS-PAGE gel.
523

524 **Protein interaction assay**

525 To explore the interaction between FtsEX and EnvC, we employed affinity chromatography with
526 TALON resin. Specifically, 15 µg of FtsEX or its ATPase-defective variants were introduced to the
527 resin pre-equilibrated at room temperature, utilizing a Micro Gravity Column, for a 15-minute
528 duration. After washing away unbound FtsEX with 100 µl of buffer E (50 mM Tris-HCl pH 8.0, 150
529 mM NaCl, 10% glycerol, and 2 mM $MgCl_2$) supplemented with 5 mM imidazole (to get rid of the
530 extra ATP present in the protein), we incorporated 5 µg of EnvC diluted in 60 µl of the
531 aforementioned buffer in the presence and absence of ATP or ATP analogs. This mixture was
532 incubated for an additional 10 minutes. Subsequently, the beads were rinsed with buffer E
533 supplemented with 5 mM imidazole in the presence and absence of ATP or ATP analogs. To elute
534 the bound proteins and possible interaction partners, we utilized 20 µl of buffer E with a
535 concentration of 300 mM imidazole, either with or without 2 mM ATP or ATP analogs. Eluted
536 proteins were then analyzed using SDS-PAGE.
537

538 To explore the interactions between FtsEX/EnvC and AmiB, 20 µg of FtsEX/EnvC or its ATPase-
539 deficient variants, $FtsE^{E163Q}X$/EnvC, were added to the TALON resin. This was done either in the
540 presence or absence of 2 mM ATP or ATP analogs and incubated at room temperature for 15
541 minutes. Any free FtsEX/EnvC or $FtsE^{E163Q}X$/EnvC was removed by washing the resin with 100 µl
542 of buffer E containing 5 mM imidazole. Following this, 10 µg of AmiB were introduced to the resin
543 with or without 2 mM ATP or ATP analogs. After a 10-minute incubation, a triple wash was executed
544 using 100 µl of buffer E supplemented with 5 mM imidazole, either with or without 2 mM ATP or
545 ATP analogs . Finally, bound proteins were eluted using 20 µl of buffer E supplemented with 300
546 mM imidazole, either with or without 2 mM ATP or ATP analogs, and the elution profile was
547 assessed via SDS-PAGE.

548

549 **Reconstitution of FtsEX complexes**

550 For the reconstitution of the FtsEX-EnvC complex, an excess of EnvC, three times the amount of
551 FtsEX, was introduced to the resin-bound FtsEX-peptidiscs during the purification process. This
552 mixture was allowed to interact at room temperature for 15 minutes. Subsequent to this incubation,
553 any free EnvC was removed by washing with buffer A containing 20 mM imidazole. The FtsEX-
554 EnvC complex was subsequently eluted from the resin using buffer A supplemented with 200 mM
555 imidazole. This eluted protein was applied to additional purification through gel filtration on a
556 Superose 6 increase 10/300 column, equilibrated in buffer B. Fractions containing the FtsEX-EnvC
557 complex were assessed using SDS-PAGE, combined, concentrated to a concentration of 3 mg/ml,
558 and stored at -80°C.

559

560 For the reconstitution of the AmiB-EnvC-FtsEX supercomplex, AmiB was mixed with the FtsEX-
561 EnvC complex in peptidiscs, at a 3:1 ratio. Following a 15-minute incubation, the supercomplex
562 was further purified via gel filtration. Fractions encompassing the FtsEX-EnvC-AmiB complex were
563 collected, concentrated to 3 mg/ml, and subsequently stored at -80°C.

564

565 **ATP hydrolysis assay**

566 To assess the ATPase activity of FtsEX and its mutants or complxes, we employed the malachite
567 green phosphate assay (40). We introduced 2 μg of FtsEX with or without 0.7 μg of EnvC or 0.7 μg
568 AmiB of following 0.8 μg of EnvC into a 20 μl reaction buffer comprising 25 mM Tris-HCl (pH 8.0),
569 150 mM NaCl, and 2 mM ATP/$MgCl_2$. For the elucidation of the Michaelis-Menten constants,
570 varying concentrations of ATP/$MgCl_2$, ranging from 0.05 to 5 mM, were utilized to initiate the
571 enzymatic reaction. After a 10-minute incubation at 37°C, 80 μl of the Malachite Green-Ammonium
572 Molybdate (MG-AG) solution was added and the resultant mixture was quickly vortexed to
573 deactivate the enzyme. A brief 2-minute incubation was followed by the addition of 10 μl of a 34%
574 (w/v) sodium citrate solution, with a subsequent vortexing step. Absorbance was then recorded at
575 650 nm after a 5-minute interval. Quantification of released inorganic phosphate (Pi) was achieved
576 using a calibration curve derived from known Pi concentrations in a K_2HPO_4 solution. Data
577 processing and curve fitting to the Michaelis-Menten equation were conducted utilizing Microsoft
578 Excel in conjunction with GraphPad Prism 9.

579

580 **Negative staining imaging of FtsE^{E163Q}X-EnvC-AmiB complex**

581 For negative staining of the FtsE^{E163Q}X-EnvC-AmiB sample, it was diluted to a concentration of
582 0.01 mg/ml. A 5 μl aliquot of the sample was deposited onto a 300 mesh copper grid coated with
583 carbon film (EMS). After allowing the sample to interact with the grid for 60 seconds, any surplus
584 was carefully blotted away using filter paper. The grid was then washed with 5 μl of Uranyless EM

585 Stain (EMS). Subsequent to the washing step, the grid was stained by applying another 5 µl of the
586 Uranyless EM Stain for 120 seconds. Excess stain was again removed with filter paper. The
587 prepared grid was left to air-dry under ambient conditions for approximately 15 minutes. Imaging
588 of the sample was executed with a Tecnai 12 microscope (FEI), operating at 120kV with a LaB6
589 source, and magnification set to 52, 000 x.
590
591 **Cryo-Electron microscopy sample preparation and data acquisition**
592 To prepare the sample, 3.5 µl of the protein sample at a concentration of 3 mg/ml was applied to
593 Quantifoil holey carbon grids (R1.2/1.3, 400 mesh) that were glow-discharged. To obtain the ATPγS
594 -bound complex, the sample was incubated at 37°C for 8 minutes with 3mM ATPγS-2mM Mg^{2+}
595 (FtsEX) or 2 mM ATP-Mg^{2+} ($FtsE^{E163Q}X$/EnvC) before freezing. The grids were blotted for 3.5-4
596 seconds with 100% relative humidity and then plunge-frozen in liquid ethane that was cooled by
597 liquid nitrogen using a Vitrobot System (Gatan).
598
599 Cryo-electron microscopy data was collected at liquid nitrogen temperature using a Titan Krios
600 electron microscope (Thermo Fisher Scientific), equipped with a K3 Summit direct electron detector
601 (Gatan) and GIF Quantum energy filter. All cryo-EM movies were recorded in counting mode with
602 SerialEM4 (41) with a slit width of 20 eV from the energy filter. Movies were acquired at nominal
603 magnifications of 81k x, which corresponded to a calibrated pixel size of 1.06 Å on the specimen
604 level. The total exposure time for each movie was 5 seconds, resulting in a total dose range of 35-
605 39 electrons per $Å^2$, fractionated into 34 frames. Additional electron microscopy data collection
606 parameters can be found in **Table supplement 3**.
607
608 **Cryo-Electron microscope image processing.**
609 For electron microscopy (EM) data processing, CryoSPARC (42) was utilized. Dose-fractionated
610 movies, captured with a K3 Summit direct electron detector, was first applied to motion correction
611 using MotionCor2 (43). A sum of all frames from each movie was generated applying a dose-
612 weighting scheme. This sum was utilized for all subsequent image-processing steps, except for
613 defocus determination. For that, CTFFIND4 (44) was used on the non-dose-weighted summed
614 images from all movie frames. The initial particle selection was achieved using the blob picker,
615 which was subsequently refined by the template picker. The steps of 2D and 3D classification, as
616 well as 3D refinement, were carried out using the "2D Classification", "Ab-initial Reconstruction",
617 and "Heterogeneous Refinement" functions. For further refinement, both the "Homogeneous
618 Refinement" and "Non-Uniform Refinement" functions were employed. The overall resolutions was
619 determined using the gold-standard Fourier shell correlation (FSC) threshold of 0.143. Lastly, the
620 local resolution was assessed via the "Local Resolution Estimation" tool.
621

622 **Model building and refinement for FtsEX and its complex with EnvC**
623 The cryo-EM maps of the ATPγS-bound FtsEX and ATP-bound FtsE^{E163Q}X/EnvC complexes were
624 resolved at resolutions of 3.7 Å and 3.4 Å, respectively, with sufficient quality to enable accurate
625 model building for the TMD domain, FtsE, and a portion of the PLD region (see **Figure supplement**
626 **3** and **Figure supplement 6** for details), leaving only the N-terminal region of FtsX, including
627 residues 1-52, not modeled.
628
629 Initial models for FtsE and FtsX were generated using the AlphaFold program (42). Subsequently,
630 the FtsEX models were rigid-body fitted into the cryo-EM map density using UCSF Chimera
631 software (45). These initial models were then refined manually within Coot (46). Restraints for
632 ATPγS were generated using the phenix_elbow program, employing its isomeric SMILES string
633 files obtained from the PDB Chemical Component Dictionary via Ligand Expo. Further refinement
634 was performed using Phenix (47), including 'minimization_global' and 'Real-space refinement'
635 protocols. Multiple rounds of manual adjustments in Coot, in conjunction with real-space refinement
636 in Phenix, were carried out to obtain the final model. Model validation was performed using
637 Ramachandran plots, MolProbity scores, and Clash scores in Phenix (47) (details provided in **Table**
638 **supplement 3**).
639
640 In the case of the FtsE^{E163Q}X/EnvC/ATP complex structure, the initial models for EnvC was derived
641 from AlphaFold (48) and our resolved FtsEX structure was used as initial model for FtsEX part.
642 These initial models were fitted into the cryo-EM map of the FtsE^{E163Q}X/EnvC/ATP complex using
643 UCSF Chimera (45). Subsequent manual adjustments were performed within Coot (46), and the
644 Glu163 was replaced with Gln. Similar to the ATPγS-containing complex, restraints for ATP were
645 generated using the phenix_elbow program. The model was refined using phenix software (47),
646 incorporating 'minimization_global' and 'Real-space refinement' procedures. The final model was
647 refined through multiple iterations of manual adjustments in Coot (46), alongside real-space
648 refinement in Phenix. Model quality assessment included Ramachandran plots, MolProbity scores,
649 and Clash scores, with detailed results provided in **Table supplement 3 (47)**.
650

651 **Acknowledgments**
652 We appreciate the contributions of Yibei Xiao and Zhaoxing Li from China Pharmaceutical
653 University, whose expertise in Mass Spectrometry greatly enhanced our research. Furthermore,
654 we thank all Luo lab members for their constructive comments throughout the course of this study.
655
656 **Funding:** This work was supported by the National University of Singapore Start-up grant to M. L.,
657 the Ministry of Education Tier 2 Grant to M.L. and L.-T. S. (MOE-T2EP30222-0015, MOE-
658 T2EP30220-0012, and T2EP30123-0017), the National Medical Research Council grant to L.-T. S.

(A-8001581-00-00), and the National Research Foundation grant to M.L. and L.-T. S. (NRF-CRP22-2019-0001 and NRFF11-2019-0005). SN was supported by MRC Doctoral Training Partnership grant MR/N014294/1 and a Medical and Life Sciences Research fund award. NB was supported by a Ph.D. studentship to the Midlands Integrative Biosciences Training Partnership (MIBTP) BBSRC grant BB/J014532/1 and by the Howard Dalton Centre at the University of Warwick under its small grant scheme award to support this work. Research in the laboratory of DR is supported by MRC grants MR/Z504245/1 and BBSRC grant BB/Y003187/1. The work in Spain is supported by grants PID2020-115331GB-100 funded by MCIN/AEI/10.13039/501100011033 and CRSII5_198737/1 by the Swiss National Science Foundation to J.A.H.

Data and materials availability: Two three-dimensional cryo-EM density maps of FtsEX and its complexes with EnvC have been deposited in the Electron Microscopy Data Bank under accession codes: EMD-37324 (ATPγS-bound FtsEX); EMD-37325(ATP-bound FtsE^{E163Q}X with EnvC). Two atomic models have been deposited in the Protein Data Bank under accession codes 8W6I (ATPγS bound FtsEX), and 8W6J (ATP-bound FtsE^{E163Q}X/EnvC). All data presented in this study are provided within the main text and supplementary materials, or readily accessible upon request.

References

1. T. Do, J. E. Page, S. Walker, Uncovering the activities, biological roles, and regulation of bacterial cell wall hydrolases and tailoring enzymes. *J Biol Chem* **295**, 3347-3361 (2020).
2. A. Typas, M. Banzhaf, C. A. Gross, W. Vollmer, From the regulation of peptidoglycan synthesis to bacterial growth and morphology. *Nat Rev Microbiol* **10**, 123-136 (2011).
3. P. D. A. Rohs, T. G. Bernhardt, Growth and Division of the Peptidoglycan Matrix. *Annu Rev Microbiol* **75**, 315-336 (2021).
4. S. Du, J. Lutkenhaus, Assembly and activation of the Escherichia coli divisome. *Mol Microbiol* **105**, 177-187 (2017).
5. S. Du, J. Lutkenhaus, At the Heart of Bacterial Cytokinesis: The Z Ring. *Trends Microbiol* **27**, 781-791 (2019).
6. J. Lutkenhaus, S. Du, E. coli Cell Cycle Machinery. *Subcell Biochem* **84**, 27-65 (2017).
7. Z. Lyu *et al.*, FtsN maintains active septal cell wall synthesis by forming a processive complex with the septum-specific peptidoglycan synthases in E. coli. *Nat Commun* **13**, 5751 (2022).
8. T. A. Cameron, W. Margolin, Insights into the assembly and regulation of the bacterial divisome. *Nat Rev Microbiol* 10.1038/s41579-023-00942-x (2023).
9. M. J. Tsang, T. G. Bernhardt, Guiding divisome assembly and controlling its activity. *Curr Opin Microbiol* **24**, 60-65 (2015).
10. M. J. Tsang, A. A. Yakhnina, T. G. Bernhardt, NlpD links cell wall remodeling and outer membrane invagination during cytokinesis in Escherichia coli. *PLoS Genet* **13**, e1006888 (2017).
11. T. Uehara, T. G. Bernhardt, More than just lysins: peptidoglycan hydrolases tailor the cell wall. *Curr Opin Microbiol* **14**, 698-703 (2011).

700 12. T. Uehara, K. R. Parzych, T. Dinh, T. G. Bernhardt, Daughter cell separation is controlled
701 by cytokinetic ring-activated cell wall hydrolysis. *EMBO J* **29**, 1412-1422 (2010).
702 13. M. Alcorlo, S. Martinez-Caballero, R. Molina, J. A. Hermoso, Regulation of Lytic
703 Machineries by the FtsEX Complex in the Bacterial Divisome. *Subcell Biochem* **99**, 285-315
704 (2022).
705 14. S. Pichoff, S. Du, J. Lutkenhaus, Roles of FtsEX in cell division. *Res Microbiol* **170**, 374-380
706 (2019).
707 15. S. Du, S. Pichoff, J. Lutkenhaus, Roles of ATP Hydrolysis by FtsEX and Interaction with FtsA
708 in Regulation of Septal Peptidoglycan Synthesis and Hydrolysis. *mBio* **11** (2020).
709 16. D. C. Yang *et al.*, An ATP-binding cassette transporter-like complex governs cell-wall
710 hydrolysis at the bacterial cytokinetic ring. *Proc Natl Acad Sci U S A* **108**, E1052-1060
711 (2011).
712 17. S. Du, S. Pichoff, J. Lutkenhaus, FtsEX acts on FtsA to regulate divisome assembly and
713 activity. *Proc Natl Acad Sci U S A* **113**, E5052-5061 (2016).
714 18. S. Du, W. Henke, S. Pichoff, J. Lutkenhaus, How FtsEX localizes to the Z ring and interacts
715 with FtsA to regulate cell division. *Mol Microbiol* **112**, 881-895 (2019).
716 19. S. J. Arends, R. J. Kustusch, D. S. Weiss, ATP-binding site lesions in FtsE impair cell division.
717 *J Bacteriol* **191**, 3772-3784 (2009).
718 20. M. Reddy, Role of FtsEX in cell division of Escherichia coli: viability of ftsEX mutants is
719 dependent on functional SufI or high osmotic strength. *J Bacteriol* **189**, 98-108 (2007).
720 21. K. L. Schmidt *et al.*, A predicted ABC transporter, FtsEX, is needed for cell division in
721 Escherichia coli. *J Bacteriol* **186**, 785-793 (2004).
722 22. J. Cook *et al.*, Insights into bacterial cell division from a structure of EnvC bound to the
723 FtsX periplasmic domain. *Proc Natl Acad Sci U S A* **117**, 28355-28365 (2020).
724 23. D. Mavrici *et al.*, Mycobacterium tuberculosis FtsX extracellular domain activates the
725 peptidoglycan hydrolase, RipC. *Proc Natl Acad Sci U S A* **111**, 8037-8042 (2014).
726 24. B. E. Rued *et al.*, Structure of the Large Extracellular Loop of FtsX and Its Interaction with
727 the Essential Peptidoglycan Hydrolase PcsB in Streptococcus pneumoniae. *mBio* **10**
728 (2019).
729 25. Y. Fu, K. E. Bruce, B. Rued, M. E. Winkler, D. P. Giedroc, 1H, 13C, 15N resonance
730 assignments of the extracellular loop 1 domain (ECL1) of Streptococcus pneumoniae D39
731 FtsX, an essential cell division protein. *Biomol NMR Assign* **10**, 89-92 (2016).
732 26. X. Xu *et al.*, Mechanistic insights into the regulation of cell wall hydrolysis by FtsEX and
733 EnvC at the bacterial division site. *Proc Natl Acad Sci U S A* **120**, e2301897120 (2023).
734 27. B. D. Corbin, Y. Wang, T. K. Beuria, W. Margolin, Interaction between cell division proteins
735 FtsE and FtsZ. *J Bacteriol* **189**, 3026-3035 (2007).
736 28. X. Ou *et al.*, ATP Can Efficiently Stabilize Protein through a Unique Mechanism. *JACS Au* **1**,
737 1766-1777 (2021).
738 29. S. Sridharan *et al.*, Proteome-wide solubility and thermal stability profiling reveals distinct
739 regulatory roles for ATP. *Nat Commun* **10**, 1155 (2019).
740 30. L. T. Sham, S. M. Barendt, K. E. Kopecky, M. E. Winkler, Essential PcsB putative
741 peptidoglycan hydrolase interacts with the essential FtsXSpn cell division protein in
742 Streptococcus pneumoniae D39. *Proc Natl Acad Sci U S A* **108**, E1061-1069 (2011).
743 31. S. C. Lee *et al.*, Nano-encapsulated Escherichia coli Divisome Anchor ZipA, and in Complex
744 with FtsZ. *Sci Rep* **9**, 18712 (2019).
745 32. S. C. Lee *et al.*, A method for detergent-free isolation of membrane proteins in their local
746 lipid environment. *Nat Protoc* **11**, 1149-1162 (2016).

747 33. E. Godino, C. Danelon, Gene-Directed FtsZ Ring Assembly Generates Constricted
748 Liposomes with Stable Membrane Necks. *Adv Biol (Weinh)* **7**, e2200172 (2023).
749 34. C. Ortiz, P. Natale, L. Cueto, M. Vicente, The keepers of the ring: regulators of FtsZ
750 assembly. *FEMS Microbiol Rev* **40**, 57-67 (2016).
751 35. P. Szwedziak, Q. Wang, T. A. Bharat, M. Tsim, J. Lowe, Architecture of the ring formed by
752 the tubulin homologue FtsZ in bacterial cell division. *Elife* **3**, e04601 (2014).
753 36. S. Rueda, M. Vicente, J. Mingorance, Concentration and assembly of the division ring
754 proteins FtsZ, FtsA, and ZipA during the Escherichia coli cell cycle. *J Bacteriol* **185**, 3344-
755 3351 (2003).
756 37. H. P. Erickson, M. Osawa, FtsZ Constriction Force - Curved Protofilaments Bending
757 Membranes. *Subcell Biochem* **84**, 139-160 (2017).
758 38. M. L. Carlson *et al.*, The Peptidisc, a simple method for stabilizing membrane proteins in
759 detergent-free solution. *Elife* **7** (2018).
760 39. G. Angiulli *et al.*, New approach for membrane protein reconstitution into peptidiscs and
761 basis for their adaptability to different proteins. *Elife* **9** (2020).
762 40. P. A. Lanzetta, L. J. Alvarez, P. S. Reinach, O. A. Candia, An improved assay for nanomole
763 amounts of inorganic phosphate. *Anal Biochem* **100**, 95-97 (1979).
764 41. D. N. Mastronarde, Automated electron microscope tomography using robust prediction
765 of specimen movements. *J Struct Biol* **152**, 36-51 (2005).
766 42. A. Punjani, J. L. Rubinstein, D. J. Fleet, M. A. Brubaker, cryoSPARC: algorithms for rapid
767 unsupervised cryo-EM structure determination. *Nat Methods* **14**, 290-296 (2017).
768 43. S. Q. Zheng *et al.*, MotionCor2: anisotropic correction of beam-induced motion for
769 improved cryo-electron microscopy. *Nat Methods* **14**, 331-332 (2017).
770 44. A. Rohou, N. Grigorieff, CTFFIND4: Fast and accurate defocus estimation from electron
771 micrographs. *J Struct Biol* **192**, 216-221 (2015).
772 45. E. F. Pettersen *et al.*, UCSF Chimera--a visualization system for exploratory research and
773 analysis. *J Comput Chem* **25**, 1605-1612 (2004).
774 46. P. Emsley, K. Cowtan, Coot: model-building tools for molecular graphics. *Acta Crystallogr*
775 *D Biol Crystallogr* **60**, 2126-2132 (2004).
776 47. P. D. Adams *et al.*, PHENIX: a comprehensive Python-based system for macromolecular
777 structure solution. *Acta Crystallogr D Biol Crystallogr* **66**, 213-221 (2010).
778 48. J. Jumper *et al.*, Highly accurate protein structure prediction with AlphaFold. *Nature* **596**,
779 583-589 (2021).

Figures

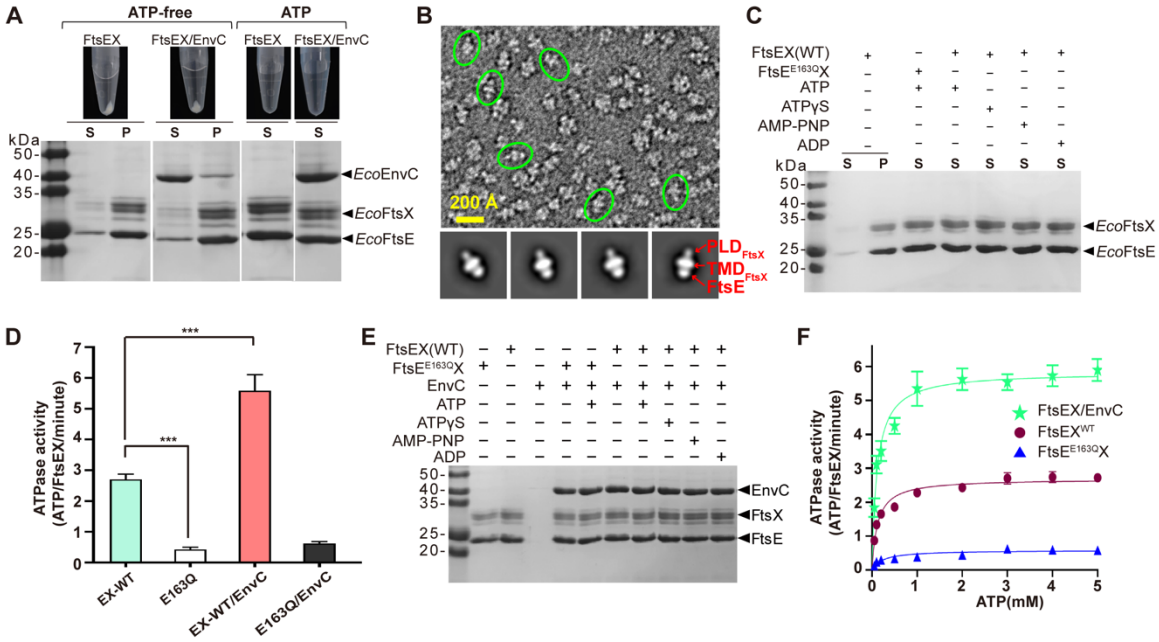

Figure 1. Biochemical reconstitution of *Eco*FtsEX and *Eco*FtsEX/EnvC complexes. (A) Evaluation of ATP's impact on FtsEX and FtsEX/EnvC complexes. Purified FtsEX and FtsEX/EnvC complexes undergo precipitation in the absence of ATP but form stable complexes when ATP is present during purification. S: Supernatant, P: Precipitate. **(B)** Representative negative staining image and 2D average of FtsEX samples purified in the presence of ATP, with FtsEX highlighted in green. The FtsE subunit, Transmembrane Domain (TMD), and Periplasmic Domain (PLD) of FtsX are clearly visible. **(C)** Assessment of ATP and ATP analogs' influence on the stability of FtsEX complex formation. ATP and ATP analogs contribute to the stabilization of the FtsEX complex. S: Supernatant, P: Precipitate. (**D**) Assessment of ATPase activity in FtsEX and FtsEX mutants, with and without EnvC. Notably, the FtsE^{E163Q}X mutants exhibit significantly reduced ATPase activity. Data represent an average of three replicates, with error bars indicating mean ± SD. Statistical analysis performed using a two-tailed unpaired t-test; ***P < 0.0005. (**E**)**.** Pull-down study illustrating EnvC binding to FtsEX or its ATPase mutant in the presence or absence of ATP or ATP analogs. The initial FtsEX or FtsE^{E163Q}X added to the resin contains 2 mM ATP, the ATP was subsequently removed by the wash buffer. (**F**) ATPase activity comparison between FtsEX and the FtsEX/EnvC complex in peptidiscs. Data represent an average of three replicates, with error bars indicating mean ± SD.

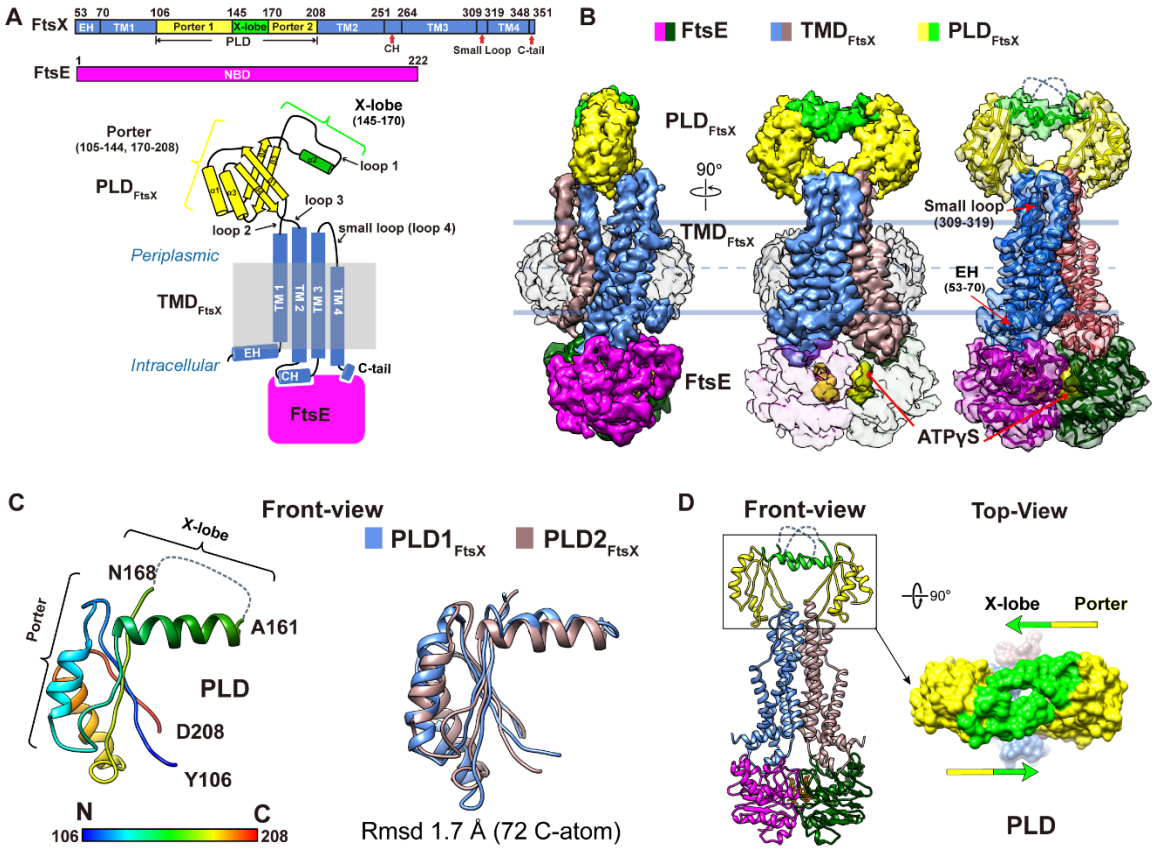

Figure 2. Cryo-EM study of *Eco*FtsEX complex in peptidiscs. (**A**) Topological diagram of FtsEX, highlighting the α helices represented as cylinders and β sheets depicted as arrows. Color scheme: FtsE (magenta and dark green), FtsX (cornflower blue), Porter of PLD_{FtsX} (yellow), and X-lobe of PLD_{FtsX} (green). CH: coupling helix, EH: elbow helix. (**B**) Left and middle panels depict the side and front views of the density map of FtsEX, with ATPγS displayed in the front view at 90% transparency. Ribbon representation of WT FtsEX in the presence of ATPγS with EM density. Color scheme: FtsE (magenta and dark green), FtsX (cornflower blue and rosy brown), Porter of PCD_{FtsX} (yellow), and X-lobe of PLD_{FtsX} (green). EH: elbow helix. (**C**) Left panel presents a rainbow representation of the PLD domain of FtsX, transitioning from blue (N-terminal) to red (C-terminal). Right panel shows a front view overlay of two PLD domains. (**D**) Surface representations of the PLD domains in a top-view configuration, with the Porter of the PLD colored in yellow and the X-lobe in green. In *Eco*FtsEX, the Porter and X-lobe are positioned facing each other.

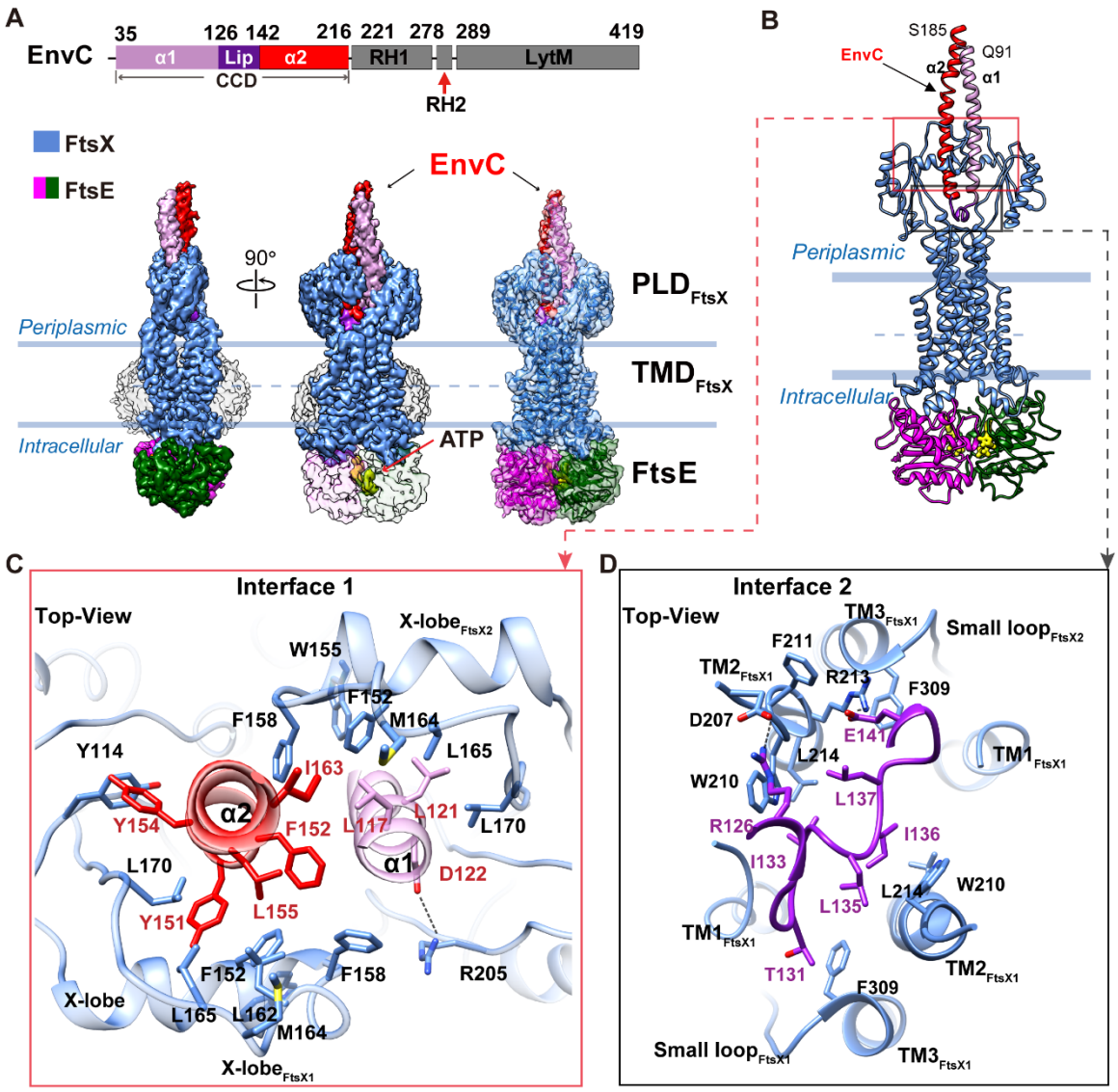

Figure 3. Cryo-EM structure of the EnvC-bound *Eco*FtsEX complex. (**A**) Domain arrangements and the overall structure of FtsEX/EnvC. Left and middle panels display side and front views of the cryo-EM density maps for FtsEX-EnvC complex in the presence of ATP. The right panel presents a ribbon representation of the structural model overlaid with the EM density. In the front-view, FtsE is depicted at 90% transparency to reveal the ATP-binding site. Color scheme of EnvC: α1 (plum), lip (purple), α2 (red), RH1, RH2, and LytM domains (grey). (**B**) EnvC binding to the PLD domain of FtsEX is depicted with ribbon representations. Color scheme: FtsX (cornflower blue), FtsE (magenta/dark green), and EnvC (red). (**C**) **&** (**D**). Top-down views provide a detailed depiction of the interaction between EnvC and FtsEX.

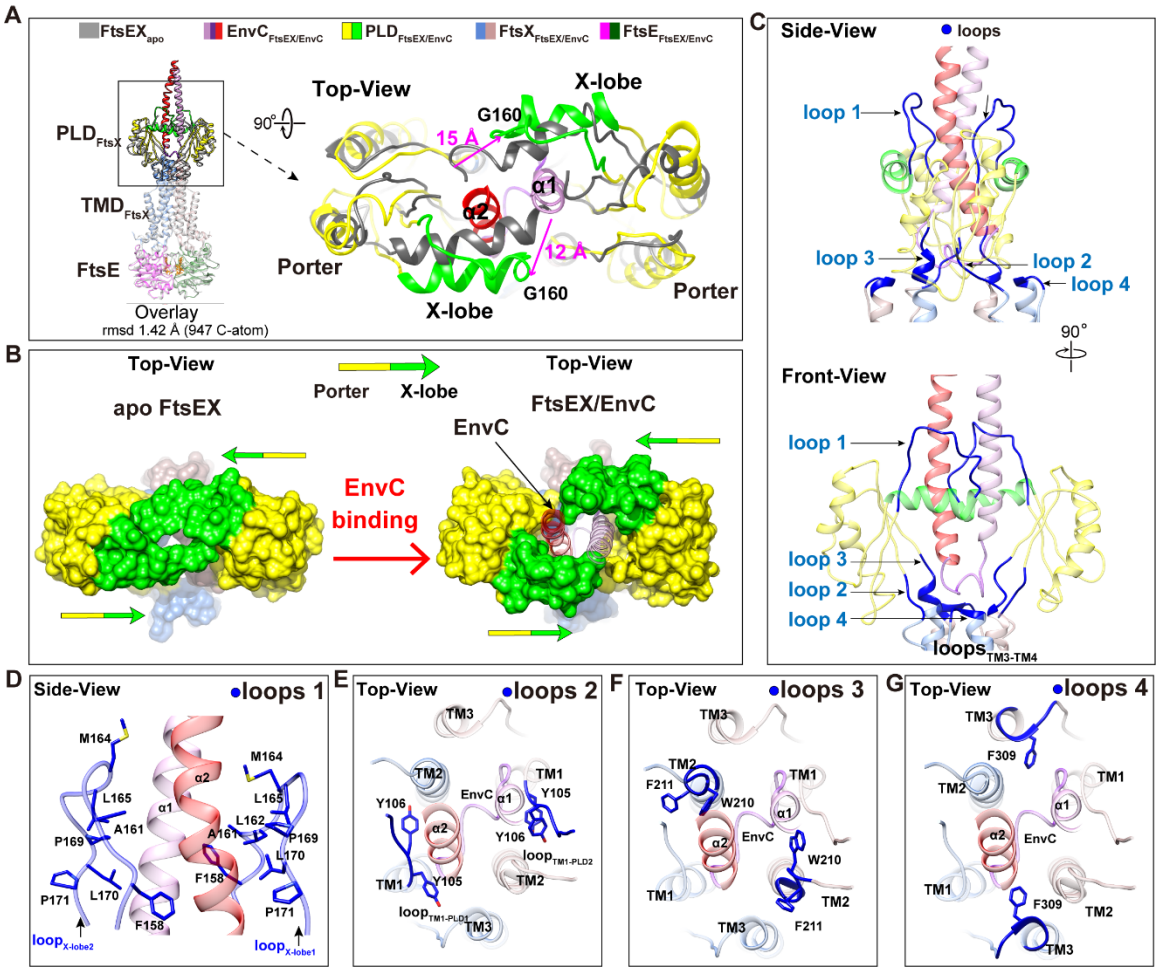

825

826 **Figure 4. Identification of key loops for EnvC binding in the *Eco*FtsEX/EnvC Complex.** (**A**)
827 Structural overlay of full-length *Eco*FtsEX and *Eco*FtsEX/EnvC complexes obtained in this study,
828 with a focus on the conformational changes in the PLD domain induced by EnvC binding. The
829 overall overlay of *Eco*FtsEX and *Eco*FtsEX/EnvC is depicted in ribbon form. Color scheme: FtsE
830 (magenta and dark green), FtsX (cornflower blue and rosy brown), Porter of PLD_{FtsX} (yellow), and
831 X-lobe of PLD_{FtsX} (green). The TMD and FtsE regions are set at 60% transparency. (**B**) Depiction
832 of the conformational changes in the PLD domains upon EnvC binding. (**C**) Side and front views
833 illustrating the key loops involved in EnvC binding within the *Eco*FtsEX/EnvC complex. Key loops
834 of FtsX, highlighted in blue, are indicated by arrows and labeled. (**D**) Side-view displaying the
835 binding details between EnvC and flexible loops located in the X-lobe (G157-L171). (**E**), (**F**), **and**
836 (**G**) Top-down views demonstrating the binding details of EnvC and flexible loops positioned
837 between TM1 and PLD (Y105-Q109) (**E**), PLD and TM2 (D208-L214) (**F**), and TM3 and TM4 (Q307-
838 T311) (**G**).
839

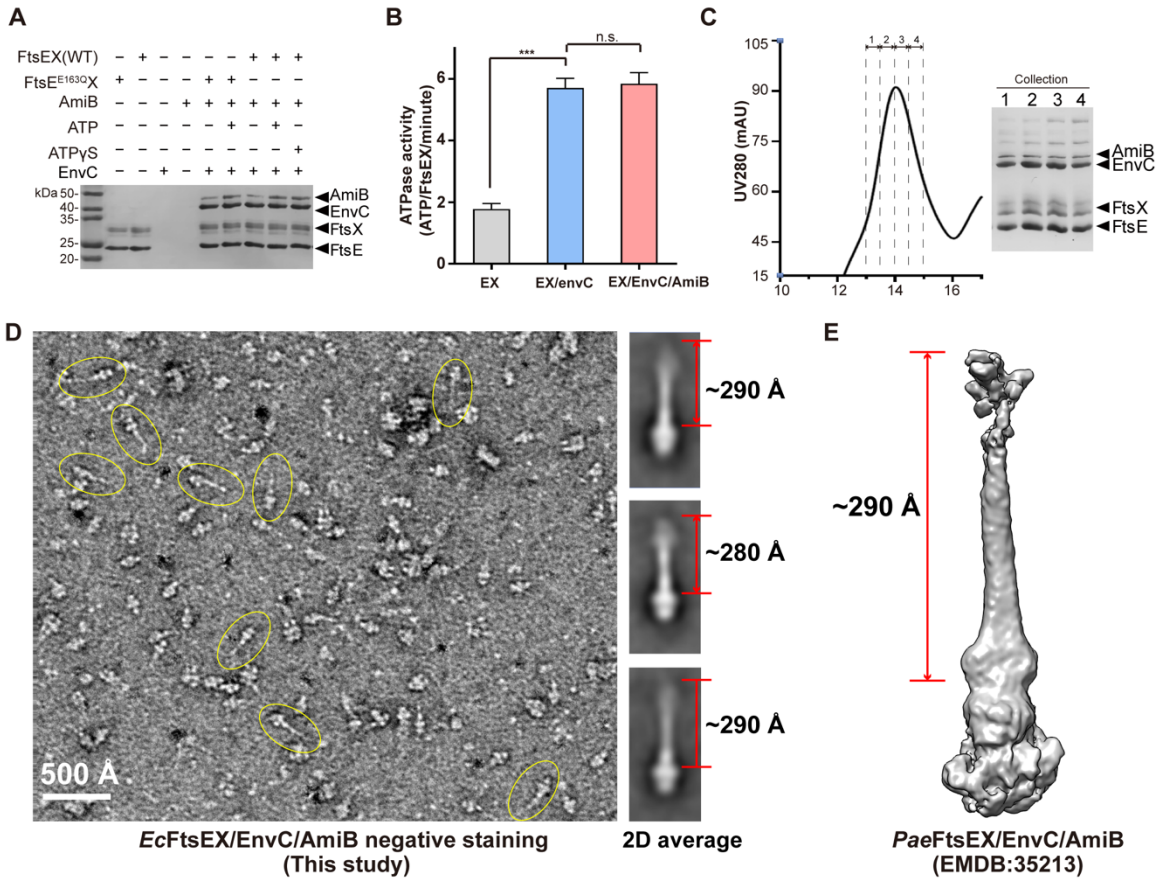

Figure 5. Biochemical reconstitution and negative-staining EM study of the AmiB-Bound *Eco*FtsEX/EnvC Complex. (**A**) Pull-down study illustrating the interaction between AmiB and FtsEX-EnvC or its ATPase mutant, in the presence or absence of ATP or its analogs. The initial FtsEX or FtsE^{E163Q}X added to the resin contains 2 mM ATP, the ATP was subsequently removed by the wash buffer. (**B**) Evaluation of ATPase activity in FtsEX, FtsEX/EnvC, and FtsEX/EnvC/AmiB complexes. Notably, the binding of AmiB does not significantly impact the ATPase activity of FtsEX/EnvC. Data represent an average of three replicates, with error bars indicating mean ± SD. Statistical analysis performed using a two-tailed unpaired t-test; ***P < 0.0005. (**C**) SEC profile and SDS-PAGE gel of purified FtsEX/EnvC/AmiB complex reconstituted in peptidiscs. (**D**) Negative-staining micrograph and 2D average image of *Eco*FtsEX/EnvC/AmiB. (**E**) Cryo-EM density map of *Pae*FtsEX/EnvC/AmiB.

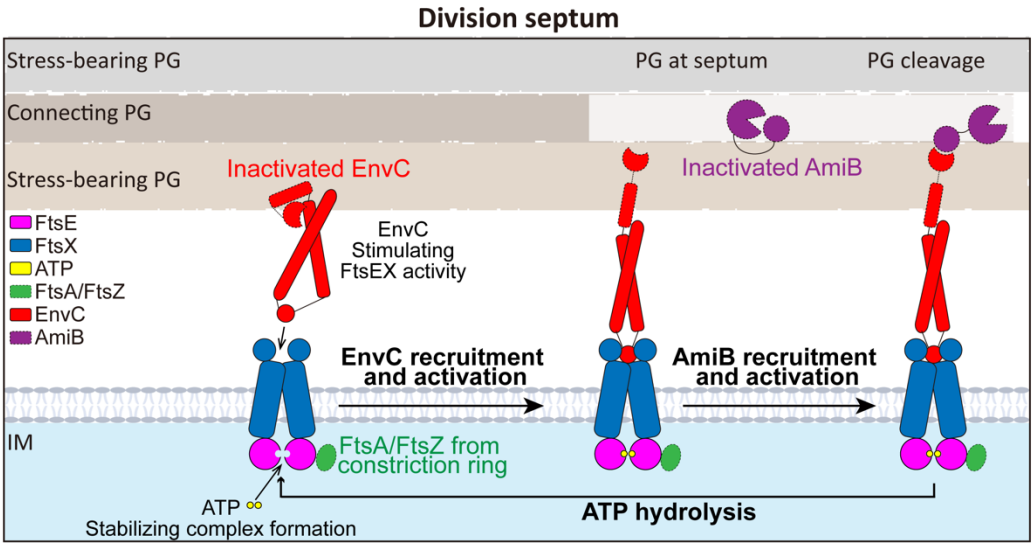

852

853 **Figure 6. A working model illustrating FtsEX complex formation, recruitment of EnvC and**
854 **AmiB, and the temporal regulation of PG cleavage activation in Gram-negative bacterial**
855 **systems.** Initially, in the cytosol, physiological ATP stabilizes the formation of the FtsEX complex,
856 while in the periplasm, the asymmetrical and inactive EnvC interacts with the flexible PLD domain
857 of FtsEX, stimulating its ATPase activity. However, the precise sequence of ATP binding and EnvC
858 recruitment in cells remains under debate. Upon complete recognition by FtsEX, the CCD domain
859 of recruited EnvC undergoes a conformational change to a symmetrical state, involving
860 compression of the coiled-coil domain, facilitating the release of the LytM domain. Interaction with
861 EnvC activates FtsEX's ATPase activity. The liberated LytM recruits amidases through direct
862 interaction with the catalytic domain's blocking helices, leading to the removal of the obstructing
863 helix from the catalytic site and activation of PG cleavage. ATP hydrolysis likely triggers the release
864 of EnvC and AmiB, allowing FtsEX to return to its normal ABC transporter state with a low basal
865 ATPase activity. The potential interaction between FtsEX and the constriction ring component
866 FtsA/FtsZ precisely locates the PG-cleaving complex at the septum for temporal regulation of PG
867 cleavage.
868